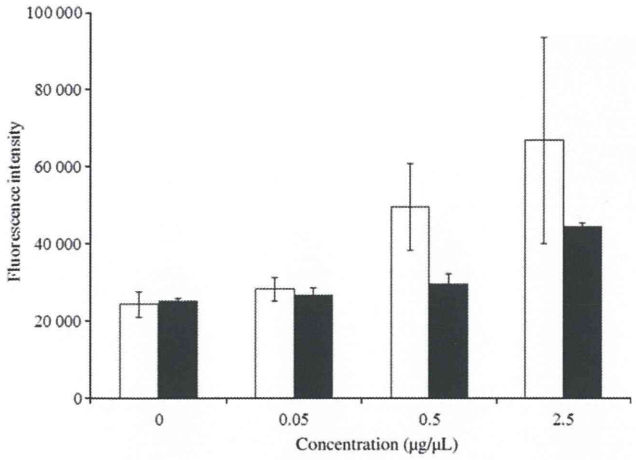

Fig. 1. Caspase-3 and caspase-7 activity in OSC-19 cells after 24 h exposure to cisplatin (CDDP) () or NC-6004 (). Caspase activity was measured using a fluorimetric assay. Values represent means ± SD from three independent experiments.

damage. The number of apoptotic cells in NC-6004-treated mice was significantly lower than that in CDDP-treated mice ($P = 0.0085$), and was similar to that in control mice (Fig. 3d). To examine functional damage, serum creatinine levels were measured. While the CDDP-treated mice showed significantly higher serum creatinine than the control group, NC-6004-treated mice showed comparable levels of serum creatinine to the control (Fig. 3e). These results indicate that NC-6004 is less toxic to the kidney than CDDP.

Efficacy of translymphatic chemotherapy and CDDP distribution in lymph nodes. To detect metastatic lymph nodes, an orthotopic xenograft mouse model of luciferase-transfected OSC-19 LN2-Luc cells was made. Primary tongue tumors were detected at the cell-inoculated site in all mice. Cervical lymph nodes were easily identified in OSC-19-inoculated mice and control mice as previously reported (Fig. 4a).[14] As it was not possible to distinguish the nodes with metastasis from the ones without metastasis macroscopically, HE and luciferase staining was performed to reveal the presence of metastases microscopically (Fig. 4b). The incidence of lymphatic metastasis was significantly lower in the NC-6004-treated group (one of eight) than that of the controls (seven of eight) and the CDDP-treated group (three of eight; $P < 0.01$; Fig. 4c). The time-course of elemental platinum (Pt) concentrations in plasma and cervical lymph nodes after sublingual injection of CDDP or NC-6004 was measured (Fig. 4d). Both plasma and lymph node concentrations after administration of NC-6004 peaked at 24 h, representing remarkably prolonged blood and lymphatic circulation; however, Pt was cleared rapidly from circulation in the CDDP group. $AUC_{0-144\ h}$ for plasma and lymph nodes in the NC-6004 group were significantly higher than those in the CDDP group. Although at day 6 (144 h) the Pt levels in plasma were undetectable in both groups, lymph nodes of the NC-6004 group still showed a high Pt concentration (1.15 ± 0.34 μg/g).

Discussion

Cancer nanotechnology is a new field of interdisciplinary research aiming to enhance the methods of cancer diagnosis and treatment.[15] From the standpoint of DDS targeting solid carcinoma, a variety of polymeric micelle-based anticancer drugs have been developed to achieve high and selective accumulation at the tumor site.[16–18] CDDP is a key drug in chemotherapy for malignancies such as lung, gastrointestinal, genitourinary and head and neck cancer.[2] Studies have shown that NC-6004 caused better selective accumulation of CDDP in tumors while lessening its distribution in normal tissue.[9] NC-6004, of which the drug-loaded core is covered by a

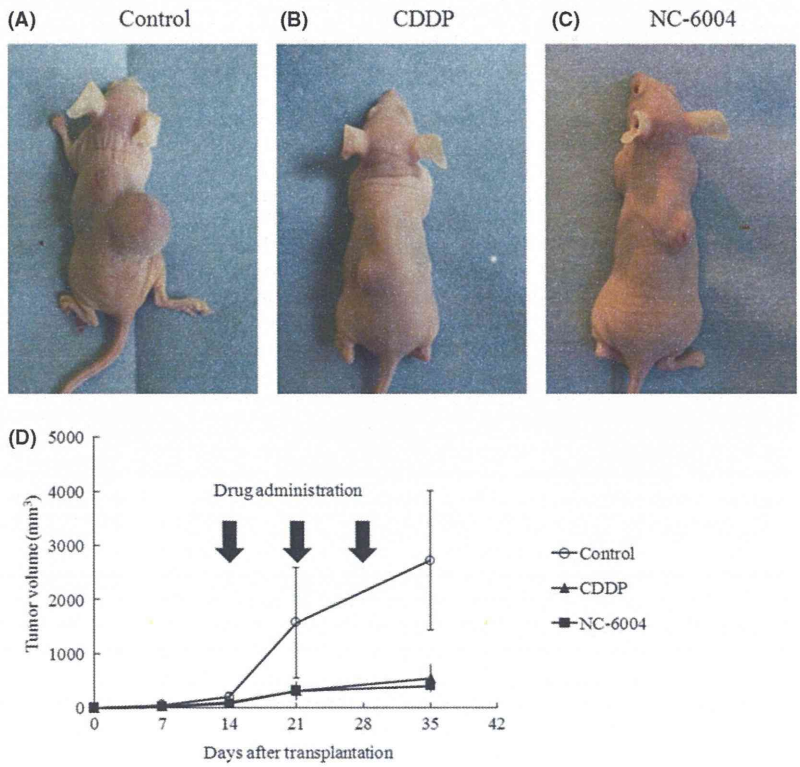

Fig. 2. Effect of cisplatin (CDDP) or NC-6004 in OSC-19 mouse models. The OSC-19 cell line was inoculated into the dorsal skin of nude mice. Photographs of representative mice and tumors treated with drugs are shown (A–C). (D) Reduced tumor volume treated with CDDP and NC-6004 relative to the control group. Each data point is the mean value (±SD) of six primary tumors.

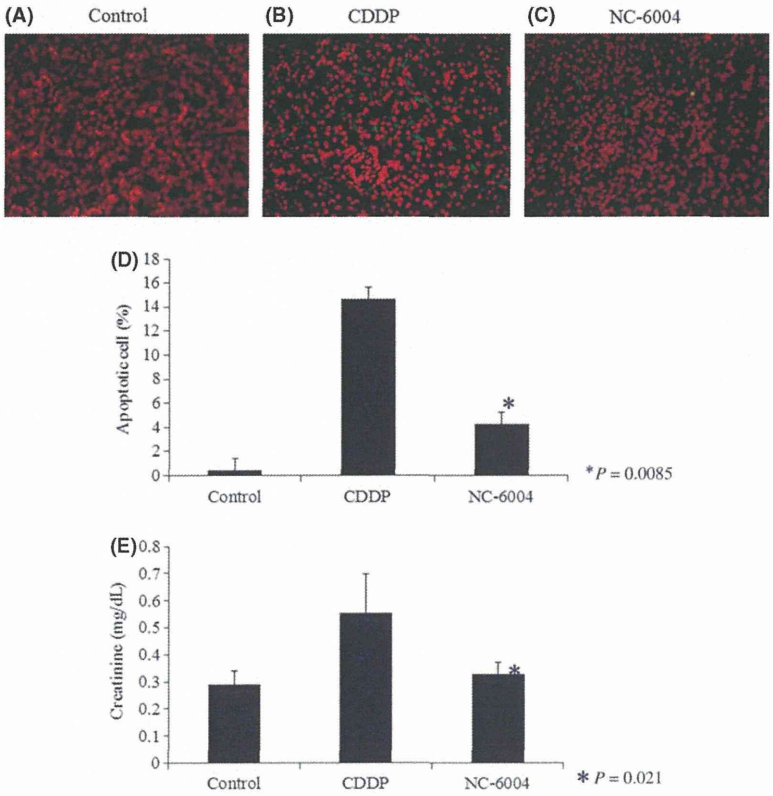

Fig. 3. Low renal toxicity of NC-6004. Mice were treated with cisplatin (CDDP) (10 mg/kg) or NC-6004 (an equivalent dose of 10 mg/kg CDDP) and kidney sections were obtained on day 28 after administration of the drug. (A–C) Immunofluorescence staining of clusters of TUNEL-positive nuclei (green) and DAPI (red). (D) The number of apoptotic cells per 100 were counted. Bars indicate standard deviations. *P = 0.0085 for CDDP versus NC-6004. Each group included five mice. (E) Plasma concentration of creatinine (mg/dL) after treatment with the control, CDDP or NC-6004. *P = 0.0021 for CDDP versus NC-6004. Each group included five mice.

hydrophilic poly(ethylene glycol) shell layer, is not detected by macrophages, can be retained in the circulation for long periods, is redistributed in tissue and can extravagate preferentially to infiltrate solid tumors. In the present study, we have investigated the antitumor properties and nephrotoxic effects of NC-6004 on human oral cancer cell lines. Moreover, a submucosal injection of NC-6004 exhibited substantial therapeutic efficacy in inhibiting cervical lymphatic metastasis in an orthotopic tongue cancer model.

To characterize the cellular basis of NC-6004 cytotoxicity relative to CDDP, we tested the two drugs in four different oral squamous carcinoma cell lines. The success of CDDP lies in its ability to arrest DNA synthesis, induce oxidative stress and activate apoptotic pathways in tumor cells.[19] The growth-inhibitory effect of NC-6004 was significantly less than that of CDDP. The different effects between these two drugs lies in the slow release of CDDP in the presence of abundant chloride ions as NC-6004 contains coordination bonds between the atoms of Pt in CDDP and the carboxylic group in the side chain,[10] which is in line with previous studies.[9,10] The caspase cascade is activated when a CDDP stimulus induces the release of cytochrome *c* from mitochondria.[20] This activation leads to an irreversible commitment to apoptotic cell death. We found that activation of caspase-3 and caspase-7 was induced in both CDDP- and NC-6004-treated OSC-19 cells.

Nephrotoxicity is one of the most significant adverse effects of CDDP.[21] CDDP accumulates in cells from all nephron segments, but is preferentially taken up by the highly susceptible proximal tubular epithelial cells, which bear the brunt of the damage. This nephrotoxicity limits the dose that can be administered and prevents the potential efficacy of CDDP.[22] The size of NC-6004 is approximately 30 nm in diameter, which is large enough to avoid renal secretion.[9] The C_{max} value for Pt concentrations in the kidney after NC-6004 administration is much lower than that of free CDDP administration.[9] In the present study, the number of apoptotic renal cells in NC-6004-treated mice was significantly lower than that in CDDP-treated mice by approximately 66% (CDDP, 14.2%; NC-6004, 4.2%). Reductions in nephrotoxicity of NC-6004 might allow patients to undergo therapy without hospitalization for hydration and the treatment of CDDP-related toxicities.[23]

We evaluated the *in vivo* antitumor activity of NC-6004 in mice. Reductions in tumor size after administration of NC-6004 or CDDP were approximately 14–20%, respectively, and were not significantly different from each other. The data obtained could be interpreted as these micelles having efficacy against oral squamous cell carcinoma cell lines similar to that of CDDP, but with much less renal toxicity toward the host.

The presence of cervical lymph node metastasis is an indicator of poor prognosis in patients with HNSCC.[24–27] Recently, the SLN has been highlighted as the lymph node that first receives lymphatic drainage from the primary site of a tumor.[28] To control lymph node metastasis, especially SLN micrometastasis in the early stages, drugs need to be delivered in tumoricidal concentrations from the site of application. The drug is highly selective depending on the size of molecule to access the lymphatic system, which was reported as the "blood–lymph barrier". The blood–lymph barrier makes conventional anticancer agents fail to effectively enter the lymphatic system.[29] The present study showed that sublingual injection of NC-6004 in an orthotopic tongue cancer mouse model significantly reduced lymphatic tumor metastasis. Moreover, a high concentration of Pt in cervical lymph nodes was maintained for at least 24 h after administration of NC-6004, whereas CDDP was not delivered to lymph nodes, which is attributable to the lymphatic drug delivery of NC-6004 from the primary tumor. These results suggest that this new drug-delivery system and the accumulation of micelles in lymph nodes are feasible for local chemotherapy targeting SLN in patients with occult lymphatic metastasis or micrometastasis.

doi: 10.1111/cas.12079

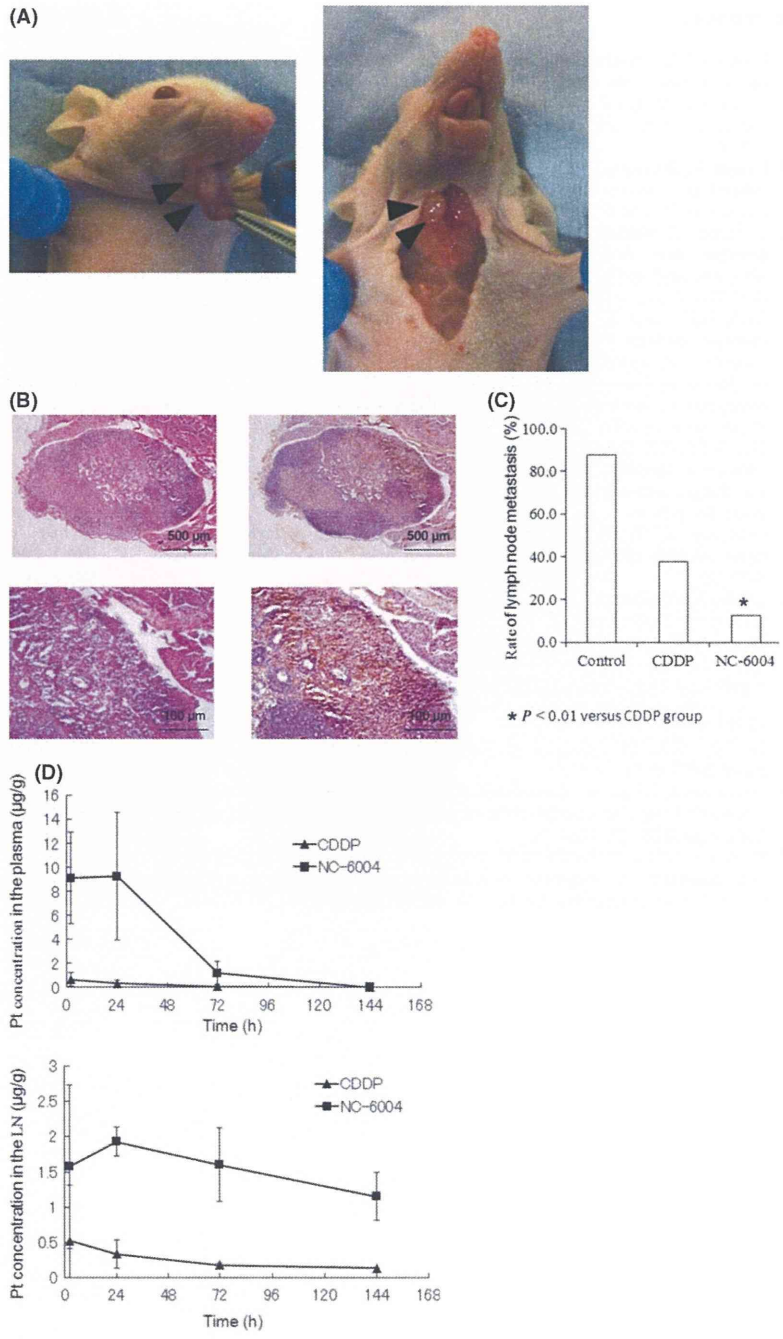

Fig. 4. Translymphatic chemotherapy targeting lymph nodes. (A) Tongue tumor and cervical lymph node metastasis of an orthotopic xenograft model. OSC-19 LN2-Luc cells were inoculated to the right side of the tongue of nude mice. Mice were killed after 35 days. A primary tumor (left, arrowhead) and cervical lymph node (right, arrowhead) were seen in the tongue. (B) Photomicrograph of lymph node metastasis. HE stain (right) and luciferase stain (left). (C) The rate of lymphatic metastasis. Each group included eight mice. (D) Time-course of elemental platinum (Pt) concentrations in plasma and cervical lymph nodes (LN) after sublingual injection of cisplatin (CDDP) (5 mg/kg) or NC-6004 (an equivalent dose of 5 mg/kg CDDP).

We did not examine Pt concentrations in cervical lymph nodes with intravenous infusion of NC-6004 and CDDP. However, Pt concentrations in the SNL were higher in the NC-6004-injected group than CDDP in topically infused groups, indicating that NC-6004 is more suitable for a lymphatic delivery system. These results suggest that such polymeric micelled-drugs, which accumulate in higher concentrations around the primary tumor than NC-6004, might be more suitable for the control of lymphatic disease in HNSCC.

The present study demonstrated the superior safety and antitumor efficacy of NC-6004 against head and neck cancer cells over that of CDDP. Considering the potential advantages in terms of noticeable antitumor activity, lymphatic drug delivery and reduced nephrotoxicity, NC-6004 represents a significant structural improvement in the development of a platinum complex. NC-6004 has progressed to a phase I clinical trial in the UK,[23] and phase I/II trials are currently underway in East Asia.

Acknowledgments

This work was supported by JSPS KAKENHI grant numbers 22791579 and 2365972, and a Grant for Clinical Cancer Research from the Ministry of Health, Labour, and Welfare of Japan.

Disclosure Statement

The authors have no conflict of interest.

References

1 Leemans CR, Braakhuis BJ, Brakenhoff RH. The molecular biology of head and neck cancer. *Nat Rev Cancer* 2011; **11**: 9–22.
2 Boulikas T, Vougiouka M. Recent clinical trials using cisplatin, carboplatin and their combination chemotherapy drugs (review). *Oncol Rep* 2004; **11**: 559–95.
3 Pinzani V, Bressolle F, Haug IJ, Galtier M, Blayac JP, Balmes P. Cisplatin-induced renal toxicity and toxicity-modulating strategies: a review. *Cancer Chemother Pharmacol* 1994; **35**: 1–9.
4 Yoshizaki T, Wakisaka N, Murono S *et al.* Intra-arterial chemotherapy less intensive than RADPLAT with concurrent radiotherapy for resectable advanced head and neck squamous cell carcinoma: a prospective study. *Ann Otol Rhinol Laryngol* 2007; **116**: 754–61.
5 Davis ME, Chen ZG, Shin DM. Nanoparticle therapeutics: an emerging treatment modality for cancer. *Nat Rev Drug Discovery* 2008; **7**: 771–82.
6 Torchilin VP. Recent advances with liposomes as pharmaceutical carriers. *Nat Rev Drug Discovery* 2005; **4**: 145–60.
7 Nishiyama N, Kataoka K. Current state, achievements, and future prospects of polymeric micelles as nanocarriers for drug and gene delivery. *Pharmacol Ther* 2006; **112**: 630–48.
8 Kataoka K, Harada A, Nagasaki Y. Block copolymer micelles for drug delivery: design, characterization and biological significance. *Adv Drug Deliv Rev* 2001; **47**: 113–31.
9 Nishiyama N, Okazaki S, Cabral H *et al.* Novel cisplatin-incorporated polymeric micelles can eradicate solid tumors in mice. *Cancer Res* 2003; **63**: 8977–83.
10 Uchino H, Matsumura Y, Negishi T *et al.* Cisplatin-incorporating polymeric micelles (NC-6004) can reduce nephrotoxicity and neurotoxicity of cisplatin in rats. *Br J Cancer* 2005; **93**: 678–87.
11 Maeda H, Sawa T, Konno T. Mechanism of tumor-targeted delivery of macromolecular drugs, including the EPR effect in solid tumor and clinical overview of the prototype polymeric drug SMANCS. *J Control Release* 2001; **74**: 47–61.
12 Sano D, Myers JN. Xenograft models of head and neck cancers. *Head Neck Oncol* 2009; **1**: 32.
13 Supavekin S, Zhang W, Kucherlapati R, Kaskel FJ, Moore LC, Devarajan P. Differential gene expression following early renal ischemia/reperfusion. *Kidney Int* 2003; **63**: 1714–24.
14 Maekawa K, Sato H, Furukawa M, Yoshizaki T. Inhibition of cervical lymph node metastasis by marimastat (BB-2516) in an orthotopic oral squamous cell carcinoma implantation model. *Clin Exp Metastasis* 2002; **19**: 513–8.
15 Manchun S, Dass CR, Sriamornsak P. Targeted therapy for cancer using pH-responsive nanocarrier systems. *Life Sci* 2012; **90**: 381–7.
16 Yokoyama M, Miyauchi M, Yamada N *et al.* Characterization and anticancer activity of the micelle-forming polymeric anticancer drug adriamycin-conjugated poly(ethylene glycol)-poly(aspartic acid) block copolymer. *Cancer Res* 1990; **50**: 1693–700.
17 Yokoyama M, Okano T, Sakurai Y, Ekimoto H, Shibazaki C, Kataoka K. Toxicity and antitumor activity against solid tumors of micelle-forming polymeric anticancer drug and its extremely long circulation in blood. *Cancer Res* 1991; **51**: 3229–36.
18 Matsumura Y. Polymeric micellar delivery systems in oncology. *Jpn J Clin Oncol* 2008; **38**: 793–802.
19 Boulikas T, Vougiouka M. Cisplatin and platinum drugs at the molecular level. (Review). *Oncol Rep* 2003; **10**: 1663–82.
20 Alnemri ES. Mammalian cell death proteases: a family of highly conserved aspartate specific cysteine proteases. *J Cell Biochem* 1997; **64**: 33–42.
21 Safirstein R, Winston J, Goldstein M, Moel D, Dikman S, Guttenplan J. Cisplatin nephrotoxicity. *Am J Kidney Dis* 1986; **8**: 356–67.
22 Townsend DM, Deng M, Zhang L, Lapus MG, Hanigan MH. Metabolism of cisplatin to a nephrotoxin in proximal tubule cells. *J Am Soc Nephrol* 2003; **14**: 1–10.
23 Plummer R, Wilson RH, Calvert H *et al.* A Phase I clinical study of cisplatin-incorporated polymeric micelles (NC-6004) in patients with solid tumours. *Br J Cancer* 2011; **104**: 593–8.
24 Leemans CR, Tiwari R, Nauta JJ, van der Waal I, Snow GB. Regional lymph node involvement and its significance in the development of distant metastases in head and neck carcinoma. *Cancer* 1993; **71**: 452–6.
25 Layland MK, Sessions DG, Lenox J. The influence of lymph node metastasis in the treatment of squamous cell carcinoma of the oral cavity, oropharynx, larynx, and hypopharynx: N0 versus N+. *Laryngoscope* 2005; **115**: 629–39.
26 Yoshizaki T, Maruyama Y, Sato H, Furukawa M. Expression of tissue inhibitor of matrix metalloproteinase-2 correlates with activation of matrix metalloproteinase-2 and predicts poor prognosis in tongue squamous cell carcinoma. *Int J Cancer* 2001; **95**: 44–50.
27 Wakisaka N, Hirota K, Kondo S *et al.* Induction of lymphangiogenesis through vascular endothelial growth factor-C/vascular endothelial growth factor receptor 3 axis and its correlation with lymph node metastasis in nasopharyngeal carcinoma. *Oral Oncol* 2012; **48**: 703–8.
28 Morton DL, Wen DR, Wong JH *et al.* Technical details of intraoperative lymphatic mapping for early stage melanoma. *Arch Surg* 1992; **127**: 392–9.
29 Grotte G, Knutson RC, Bollman JL. The diffusion of dextrans of different molecular sizes to lymph and urine. *J Lab Clin Med* 1951; **38**: 577–82.

doi: 10.1111/cas.12079

Send Orders for Reprints to reprints@benthamscience.net

14 *The Open Otorhinolaryngology Journal*, 2013, 7, 14-18

Open Access

Sentinel Lymph Node Detection in Patients with Oral Cancer by MR Lymphography using Superparamagnetic Iron Oxide

Hirokazu Uemura[1,3], Ichiro Ota[*,2], Takashi Fujii[3], Motoyuki Suzuki[3], Mio Sakai[4], Katsuyuki Nakanishi[4], Yasuhiko Tomita[5], Atsushi Noguchi[6], Hiroshi Hosoi[2] and Kunitoshi Yoshino[3]

[1]*Department of Otorhinolaryngology, Saiseikai Chuwa Hospital, Japan;* [2]*Department of Otolaryngology-Head and Neck Surgery, Nara Medical University, Japan; Departments of* [3]*Head and Neck Surgery,* [4]*Radiology,* [5]*Pathology and* [6]*Nuclear Medicine, Osaka Medical Center for Cancer and Cardiovascular Diseases, Japan*

Abstract: The purpose of this study was to examine the feasibility of interstitial MR lymphography using Superparamagnetic Iron Oxide (SPIO) to detect sentinel lymph nodes (SLNs) in head and neck cancer. For two patients with cT2N0 squamous cell carcinoma of the tongue, the submucosal injection of SPIO as well as sentinel lymph node navigation surgery (SLNNS) was performed before undergoing surgical treatment. SPIO was used for MR lymphography and Tc-99m phytate for SPECT. We compared the images by both modalities. Berlin blue stain was also performed postoperatively to verify if SLNs had the uptake of SPIO. The lymph nodes with MR signal attenuation and those with hot spots were probed to be anatomically identical. All the lymph nodes detected as a SLN by a gamma-probe contained the blue granules from SPIO. These data suggest that SPIO can be a novel tracer for performing SLNNS and SLN biopsy (SLNB) in oral cancer patients with cN0 neck.

Keywords: Head and neck cancer, sentinel lymph node, superparamagnetic iron oxide, MR lymphography.

INTRODUCTION

The sensitivity for detecting lymphatic metastasis in patients with head and neck cancer as well as melanoma and breast carcinoma has significantly increased by the use of sentinel lymph node biopsy (SLNB) [1-4]. However, SLNB in head and neck cancer is not widely accepted in Japan so far. Recently, a retrospective study on sentinel lymph node for oral and laryngopharyngeal cancer in Japan was reported [5]. Indocyanine Green (ICG) is widely used for detecting sentinel lymph nodes (SLNs) in patients with head and neck cancer or breast cancer. In addition, lymphoscintigraphy is also used for detecting SLNs in the head and neck region.

ICG is such a small weight molecule that it can reach sentinel lymph nodes rapidly after injection around the primary tumors. Constant experience on the procedure of SLNB is necessary in order to identify and pick up the SLNs accurately. It should be difficult to search the whole neck extensively for the SLNs with ICG, while SPECT helps us identify the locations of them. Recently, the new imaging technique, such as near-infrared fluorescence imaging, may compensate the disadvantage with ICG [6-8], but it is still difficult to survey the whole neck for SLNs. Therefore, SPECT is often used at the same time with ICG for detecting SLNs.

SPIO, a negative contrast enhancing agent, can be one of the alternatives of SLNs identification. A magnetometer for SPIO in SLNs is available nowadays [9, 10], but the comparison between distribution of SPIO by its submucosal injection and that of radioisotope labeled agents remains unclear. In the current study we examined the feasibility of interstitial MR lymphography using SPIO to detect SLNs in 2 patients with oral cancer.

*Address correspondence to this author at the Department of Otolaryngology-Head and Neck Surgery, Nara Medical University, 840 Shijo-cho, Kashihara, Nara 634-8522, Japan; Tel: +81-744-29-8887; Fax: +81-744-24-6844; E-mail: iota@naramed-u.ac.jp

MATERIALS AND METHODS

Patients

This study was approved by the Institutional Review Board of Osaka Medical Center for Cancer and Cardiovascular Diseases. Two patients with cT2N0 squamous cell carcinoma of the tongue were enrolled as the subjects of this study. Written informed consent for this study was obtained from them. They consented to the submucosal injection of SPIO as well as to sentinel lymph node navigation surgery (SLNNS) at Osaka Medical Center for Cancer and Cardiovascular Diseases. Tc-99m phytate was used as a tracer in SLNNS.

Superparamagnetic Iron Oxide (SPIO)

Risovist® was submucosally injected around the primary tumors. It was approved in Japan in 2001 as a SPIO formulation that targeted the liver reticuloendotherial system. SPIO particles are phagocytosed by reticuloendothelial cells in the liver, resulting in negative enhancement of the liver parenchyma on T2- or T2*-weighted imaging. The iron oxide core is about 5 nm in diameter. It is coated with carboxydextran and clustered. The size of particles is 57 nm respectively. The SPIO particles bind with opsonins in the vessels and about 80% of dosage is

1874-4281/13

phagocytosed by Kupffer cells in the liver reticuloendotherial system. The SPIO particles accumulate in the lysosome granules and form cluster in the Kupffer cell, the large clusters disturb local magnetic field, shortens T2 * and decrease the signal strength of the liver. Moreover, small clusters assume the approach of the water molecule to magnetic center to be easy, and shortens T1 and T2. The decreased or increased signal strength of the liver results in improvement of neoplasm-liver contrast and it contributes to the diagnosis of the liver tumors.

The SPIO particles are phagocytosed by macrophages in lymph nodes. Therefore, the decrease of signal strength also occurs in the lymph nodes with uptake of SPIO.

Injection of SPIO

Undiluted solution of Risovist® was submucosally injected with the dose of 0.45mg/kg (= 8μmol Fe/kg, < 1.4ml/body). The mucosa around tumor was not pretreated with any local anesthetics but patients complained of no severe pain. Risovist® was injected in surroundings of the primary lesion one fourth of the volume of SPIO each.

SPIO Contrast Enhanced MRI

MRI was performed twice before and 30 minute after the submucosal injection of SPIO. MRI images were evaluated for the lymph nodes with attenuation of signal strength. Both MRI images of the pre- and post-injection were compared with each other if the lymph nodes detected by MRI anatomically coincided to SLNs detected by SPECT.

Detection and Removal of SLNs During Surgical Treatment

The flowchart about imaging studies and surgical treatment for the patients was shown in Fig. (**1**). We intraoperatively used the gamma probe (Neo2000 Gamma Detection System, Mammotome, Cincinnati, OH) to locate the SLNs with Tc-99m phytate. The lymph nodes with the counts of ten times as much as those of the back ground values were defined as the SLNs. These lymph nodes were immediately evaluated to verify if there was an evidence of microscopical metastasis by the frozen section when removed. The iron staining with berlin blue was done to the permanent preparation to confirm the existence of iron in the SLNs.

RESULTS

The lymph nodes that accumulated SPIO located in the same anatomical positions where the hot spots with accumulation of Tc-99m phytate were identified by SPECT in both Case 1 and Case 2. These data imply that both of them turned out to be anatomically identical (Figs. **2**, **3**).

To detect SLNs with SPIO, but the removed SLNs were treated with berlin blue stain, instead of the using a magnetometer intraoperatively [9, 10]. The blue granules shown in Fig. (**4**) indicated the uptake of SPIO in the sinus of SLNs. All the lymph nodes detected as a SLN by a gamma-probe contained those blues granules.

DISCUSSION

Organ preservation is an important goal in treatment for head and neck cancer, and the modalities such as chemoradiation aiming at coexisting of that purpose and the therapeutic effect are widely adopted. Minimum surgical stress is expected because excellent prognosis is obtained by surgical treatment for early cancer of tongue even though the potential of cervical lymph node metastasis in cN0 neck is focused on in T1/T2 tumors. To overcome this task, the clinical researches on SLNs in the oral cavity cancer are ongoing [5, 7, 11].

ICG is widely used to identify SLNs intraoperatively. ICG can run rapidly through the lymphatic drainage system because its particle is small. Therefore, we need to become more experienced on SLNNS or SLNB with ICG. In addition, it is low-priced and the procedure is clear. This is why ICG is still used for SLNNS or SLNB for head and neck cancer. Recently, Photodynamic Eye (PDE) and ICG is an effective combination in order to visualize tissue perfusion and SLNs [8]. We can also use a transparent hemispherical device that is effective in order to identify the lymph nodes in the deep part of the neck by shortening the distance from the skin to the target [8].

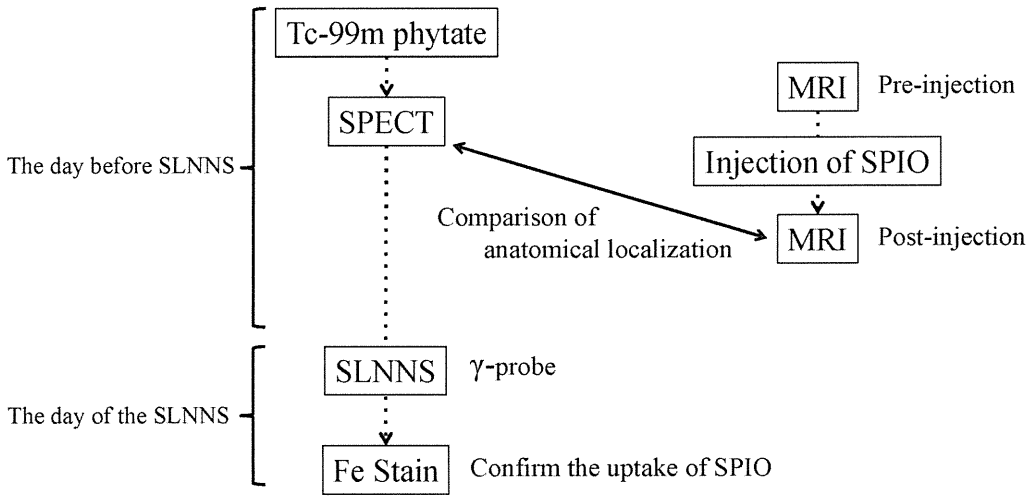

Fig. (1). The flowchart for imaging studies and SLNNS.

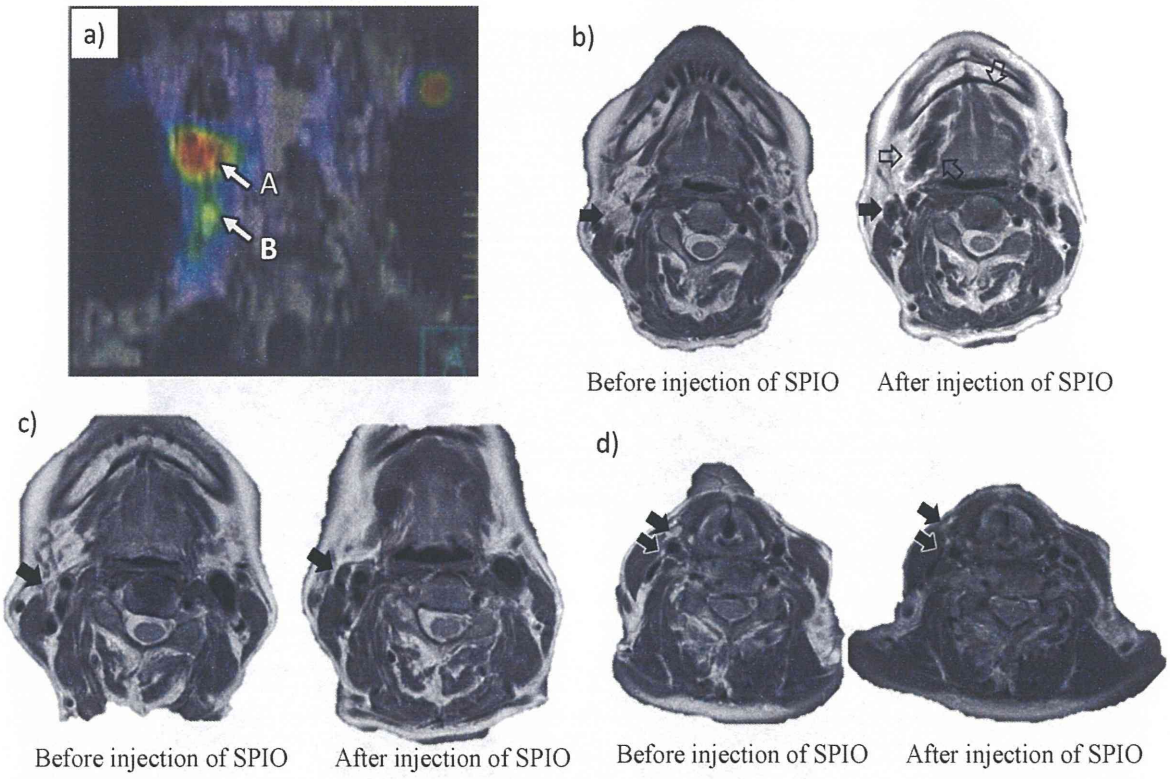

Fig. (2). Case1; **a)** The locations of SLNs were identified by SPECT. **b** and **c)** The signal attenuation was shown by MRI (T2W, closed arrows). SPIO around the primary lesion was surrounded by open arrows. Those lymph nodes anatomically coincided with the hot spot A in photo a. **d)** Other lymph nodes with signal attenuation were detected by MRI (T2W, closed arrows). They were anatomically coincided with the lower part of hot spot B in photo a.

CT lymphangiography is one of the useful identification methods for the sentinel lymph nodes and the descriptions such as MPR and 3D are easy to understand anatomically. Saito *et al.* reported the lateral lingual lymph node that was identified as a sentinel node demonstrated on CT lymphography [10, 12]. However, the timing is the key to image SLNs appropriately, as the CT contrast agent runs through the tissues in several minutes. But other modalities such as ICG method are necessary for identifying the location of SLNs during surgical operation as well.

Even with clear laterality of head and neck primary lesions, SNLs might be in the contralateral neck. Thinking of possibility that unexpected SLNs exist as previously mentioned, an isotope method has the advantage of the whole neck scan. However, there should be various methods for identifying the location of SLNs as not all of institutions can perform SPECT.

SLNs detection using SPIO is not one of the most accepted methods so far. SPIO has some problems to solve such as high price, side effects and so on. Mack *et al.* reported evaluation of neck metastasis by MRI with ultrasmall SPIO (USPIO) injected intravenously [13]. According to the report, MR diagnosis was correct in 26 of 27 patients who underwent surgery. Harisinghani *et al.* reported the evaluation of nodal metastasis in prostatic cancer patients by MRI with intravenous USPIO injection as well [14]. And they mentioned that MRI with USPIO correctly identified all patients with nodal metastases, and a node-by-node analysis had a significantly higher sensitivity than conventional MRI. Only a few were reported about submucosal injection of SPIO and its distribution [11, 15].

This study showed that the lymph nodes detected by MRI anatomically coincided to SLNs detected by SPECT. The uptake of SPIO in the sinus of the SLNs was pathologically proved by Fe stain. Thus, MRI using SPIO submucosal injection could detect the identical lymph nodes that were detected by SPECT.

Performing MRI before and after submucosal injection of SPIO is a complicated process. SPIO is high-priced as well. It is also expected that a precise magnetometer becomes affordable and common. Interstitial MR lymphography using SPIO is thought to be feasible for detecting SLNs in head and neck cancer patients even though there are some problems to solve for now.

CONCLUSION

We evaluated images of interstitial MR lymphography with SPIO in oral cancer patients who also underwent lymphoscintigraphy. The lymph nodes that accumulated SPIO were identical to those detected by SPECT using Tc-99m phytate. SPIO can be a novel tracer for performing SLNNS and SLNB in patients with oral cancer even though it is necessary to overcome several problems.

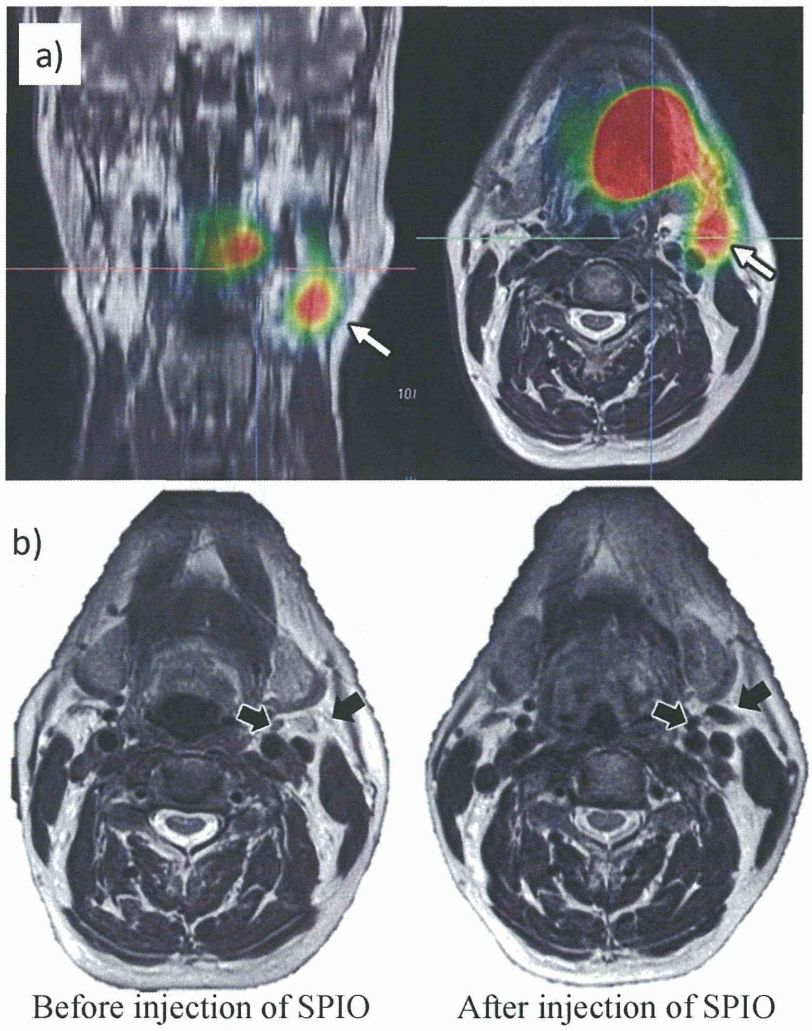

Fig. (3). Case2; **a)** The location of SLNs was identified in the left upper neck by SPECT (open arrows). **b)** The signal attenuation was shown by MRI (T2W, closed arrows). The area with decreased signal was anatomically coincided with the hot spot in photo a.

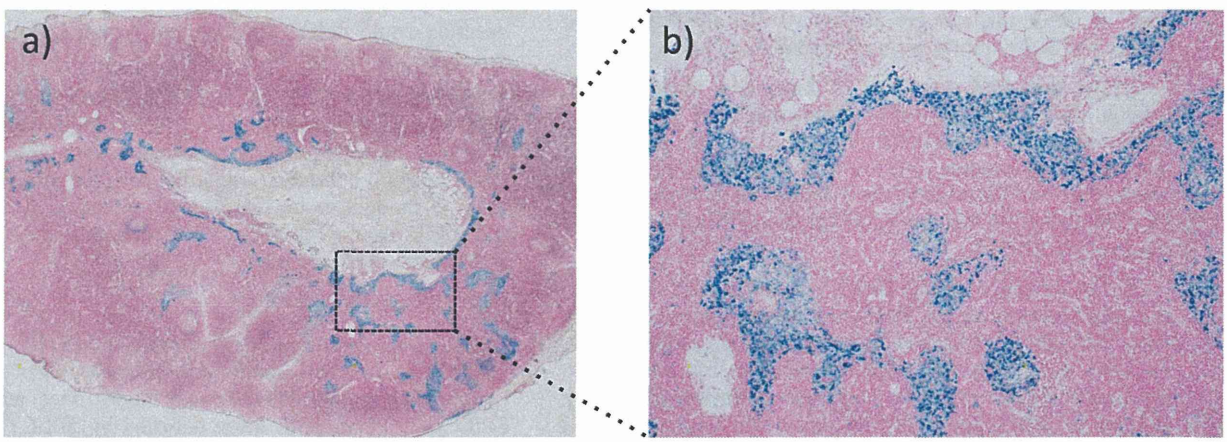

Fig. (4). A section of the lymph node detected as a SLN by a gamma-probe in Case 1. Berlin blue stain dyes iron blue in the tissue. The photos (**a**: x20; **b**: x100) show that the blue granules in sinuses are SPIO particles phagocytosed in the node.

CONFLICT OF INTEREST STATEMENT

The authors confirm that this article content has no conflict of interest.

ACKNOWLEDGEMENTS

This study was partially supported by the grant of Osaka Foundation for the Prevention of Cancer and Cardiovascular Diseases as well as the Ministry of Health, Labour and Welfare, Grant-in-Aid for Scientific Research, 2009-2011 (201119016).

REFERENCES

[1] McMasters KM, Reintgen DS, Ross MI, *et al.* Sentinel lymph node biopsy for melanoma: controversy despite widespread agreement. J Clin Oncol 2001; 19: 2851-5.

[2] Krag DN, Weaver DL, Alex JC, *et al.* Surgical resection and radiolocalization of the sentinel lymph node in breast cancer using a gamma probe. Surg Oncol 1993; 2: 335-9; discussion 340.

[3] Giuliano AE, Kirgan DM, Guenther JM, *et al.* Lymphatic mapping and sentinel lymphadenectomy for breast cancer. Ann Surg 1994; 220: 391-8; discussion 398-401.

[4] Civantos FJ, Zitsch RP, Schuller DE, *et al.* Sentinel lymph node biopsy accurately stages the regional lymph nodes for T1-T2 oral squamous cell carcinomas: results of a prospective multi-institutional trial. J Clin Oncol 2010; 28: 1395-400.

[5] Yoshimoto S, Hasegawa Y, Matsuzuka T, *et al.* Sentinel node biopsy for oral and laryngopharyngeal squamous cell carcinoma: a retrospective study of 177 patients in Japan. Auris Nasus Larynx 2012; 39: 65-70.

[6] Ogasawara Y, Ikeda H, Takahashi M, *et al.* Evaluation of breast lymphatic pathways with indocyanine green fluorescence imaging in patients with breast cancer. World J Surg 2008; 32: 1924-9.

[7] Yamauchi K, Nagafuji H, Nakamura T, *et al.* Feasibility of ICG fluorescence-guided sentinel node biopsy in animal models using the HyperEye Medical System. Ann Surg Oncol 2011; 18: 2042-7.

[8] Tagaya N, Nakagawa A, Abe A, *et al.* Non-invasive identification of sentinel lymph node using indocyanine green fluorescence imaging in patients with breast cancer. Open Surg Oncol J 2010; 2: 71-4.

[9] Minamiya Y, Ito M, Katayose Y, *et al.* Intraoperative sentinel lymph node mapping using a new sterilizable magnetometer in patients with nonsmall cell lung cancer. Ann Thorac Surg 2006; 81: 327-30.

[10] Shiozawa M, Lefor AT, Hozumi Y, *et al.* Sentinel lymph node biopsy in patients with breast cancer using superparamagnetic iron oxide and a magnetometer. Breast Cancer 2013; 20: 223-9.

[11] Mizokami D, Kosuda S, Tomifuji M, *et al.* Superparamagnetic iron oxide-enhanced interstitial magnetic resonance lymphography to detect a sentinel lymph node in tongue cancer patients. Acta Otolaryngol 2013; 133: 418-23.

[12] Saito M, Nishiyama H, Oda Y, *et al.* The lingual lymph node identified as a sentinel node on CT lymphography in a patient with cN0 squamous cell carcinoma of the tongue. Dentomaxillofac Radiol 2012; 41: 254-8.

[13] Mack MG, Balzer JO, Straub R, *et al.* Superparamagnetic iron oxide-enhanced MR imaging of head and neck lymph nodes. Radiology 2002; 222: 239-44.

[14] Harisinghani MG, Barentsz J, Hahn PF, *et al.* Noninvasive detection of clinically occult lymph-node metastases in prostate cancer. N Engl J Med 2003; 348: 2491-9.

[15] Ishiyama K, Motoyama S, Tomura N, *et al.* Visualization of lymphatic basin from the tumor using magnetic resonance lymphography with superparamagnetic iron oxide in patients with thoracic esophageal cancer. J Comput Assist Tomogr 2006; 30: 270-5.

Received: November 27, 2013 Revised: December 4, 2013 Accepted: December 5, 2013

Ann Surg Oncol (2012) 19:3865–3870
DOI 10.1245/s10434-012-2409-0

Annals of
SURGICAL ONCOLOGY
OFFICIAL JOURNAL OF THE SOCIETY OF SURGICAL ONCOLOGY

ORIGINAL ARTICLE – HEAD AND NECK ONCOLOGY

Intraoperative Molecular Assessment for Lymph Node Metastasis in Head and Neck Squamous Cell Carcinoma Using One-Step Nucleic Acid Amplification (OSNA) Assay

Takashi Matsuzuka, MD, PhD[1], Katsumasa Takahashi, MD, PhD[2], Daisuke Kawakita, MD, PhD[3], Naoyuki Kohno, MD, PhD[4], Hiroshi Nagafuji, MD[4], Koichi Yamauchi, MD, PhD[4], Masahiro Suzuki, MD[1], Tomohiro Miura, MD, PhD[1], Nobuhiko Furuya, MD, PhD[2], Yasushi Yatabe, MD, PhD[5], Keitaro Matsuo, MD, PhD, MSc[3], Koichi Omori, MD, PhD[1], and Yasuhisa Hasegawa, MD, PhD[6]

[1]Department of Otolaryngology, Fukushima Medical University School of Medicine, Fukushima, Japan; [2]Department of Otolaryngology-Head and Neck Surgery, Gunma University Graduate School of Medicine, Maebashi, Japan; [3]Division of Epidemiology and Prevention, Aichi Cancer Center Research Institute, Nagoya, Japan; [4]Department of Otolaryngology-Head and Neck Surgery, Kyorin University School of Medicine, Mitaka, Japan; [5]Department of Pathology and Molecular Diagnosis, Aichi Cancer Center Hospital, Nagoya, Japan; [6]Department of Head and Neck Surgery, Aichi Cancer Center Hospital, Nagoya, Japan

ABSTRACT

Background. Conventional intraoperative pathological examination for Sentinel node navigation surgery (SNNS) has been controversial. We evaluated the efficacy of one-step nucleic acid amplification (OSNA) assay for intraoperative diagnosis of cervical lymph node (CLN) metastasis compared with histopathological examination in patients with head and neck squamous cell carcinoma (HNSCC).

Methods. A total of 175 CLNs dissected from 56 patients with HNSCC who underwent surgery at Aichi Cancer Center, Kyorin University, Gunma University or Fukushima Medical University, between April 2008 and December 2011 were enrolled. CLN samples were sectioned into four equal pieces, with two of each used for OSNA assay and other histopathological examinations. The diagnostic value of OSNA assay in HNSCC patients in predicting the results of histopathological diagnosis was evaluated using the area under the receiver operating characteristic (AUROC) curve.

Results. OSNA assay showed acceptable efficacy in the detection of pathological CLN metastasis (AUROC 0.918, 95 % confidence interval [CI] 0.852–0.984). Regarding the CK19mRNA cutoff value, the optimum cutoff point in HNSCC patients was 131 copies/μl (sensitivity: 82.4, 95 % CI 65.5–93.2; specificity: 99.3, 95 % CI 96.1–100.0; positive likelihood ratio 116.1; negative likelihood ratio 0.2].

Conclusions. We demonstrated that OSNA assay is useful in intraoperative diagnosis for CLN metastasis in patients with HNSCC. OSNA assay could be applied for SNNS in HNSCC patients.

The trend to minimally invasive surgery (MIS), which is now commonly used for various types of diseases, is motivated by the pursuit of fewer intra- and post-operative complications. Sentinel node navigation surgery (SNNS) is mainly used in patients with breast cancer and skin melanoma. The sentinel node (SLN) refers to the first lymph node draining from the primary region of the cancer, and SLN biopsy (SLNB) aids in the detection of occult metastasis in early-stage cancer. The idea behind the SLN concept is that it allows the detection of clinically occult node metastases that cannot be detected by imaging. When

Takashi Matsuzuka, Katsumasa Takahashi, Daisuke Kawakita and Naoyuki Kohno contributed equally to this work, and all should be considered first author.

Electronic supplementary material The online version of this article (doi:10.1245/s10434-012-2409-0) contains supplementary material, which is available to authorized users.

First Received: 28 February 2012;
Published Online: 23 May 2012

Y. Hasegawa, MD, PhD
e-mail: hasegawa@aichi-cc.jp

metastasis is not detected in SLNs, lymph node dissection is avoidable.[1] The concept of SNNS has been extended to cancers other than breast cancer, including head and neck squamous cell carcinoma (HNSCC).[2–14]

The objective standard of intraoperative detection of metastasis from the SLN is pathological examination of frozen sections. A major difficulty with this approach is maintaining diagnostic accuracy within the limited time of the operative procedure. In fact, the reported sensitivity of frozen-section diagnosis compared with final pathological results in patients with HNSCC ranges from 60 to 70 %, mainly as a result of the failure to detect micrometastasis.[8,9,15,16]

One means of overcoming this problem is one-step nucleic acid amplification (OSNA) assay (Sysmex, Kobe, Japan), a rapid and semiquantitative intraoperative procedure for detecting cytokeratin 19 (CK 19) mRNA in lymph nodes in SNNS.[17] This method has been found to be efficacious in multicenter clinical trials for breast cancer, gastric cancer, and colorectal cancer.[18–22] To our knowledge, however, the clinical efficacy of OSNA assay in HNSCC has not been evaluated.

Here, we conducted a multi-institutional prospective cohort study to evaluate the efficacy of OSNA assay for intraoperative diagnosis of cervical lymph node (CLN) metastasis in comparison with histopathological diagnosis in HNSCC patients.

MATERIALS AND METHODS

Patients

A total of 56 HNSCC patients with 175 CLNs dissected during surgery at Aichi Cancer Center, Kyorin University, Gunma University and Fukushima Medical University, between April 2008 and December 2011 were enrolled. Inclusion criteria were no history of cancer, histological diagnosis of squamous cell carcinoma, and no distant metastasis. Patients who had received neoadjuvant treatment were excluded. This study was approved by the ethics committees of all institutions involved, and all participants provided written informed consent.

CLN Processing

All CLNs obtained during surgery were collected, and sectioned into four equal pieces (a–d in Fig. 1a). Two of these pieces (a, c) were stored at −80°C until OSNA assay. The remaining two pieces (b, d) were frozen in liquid nitrogen and a pair of sections were obtained from each. One of the paired sections was then stained with hematoxylin and eosin. These stained sections were also examined immunohistochemically with cytokeratin AE1/3.

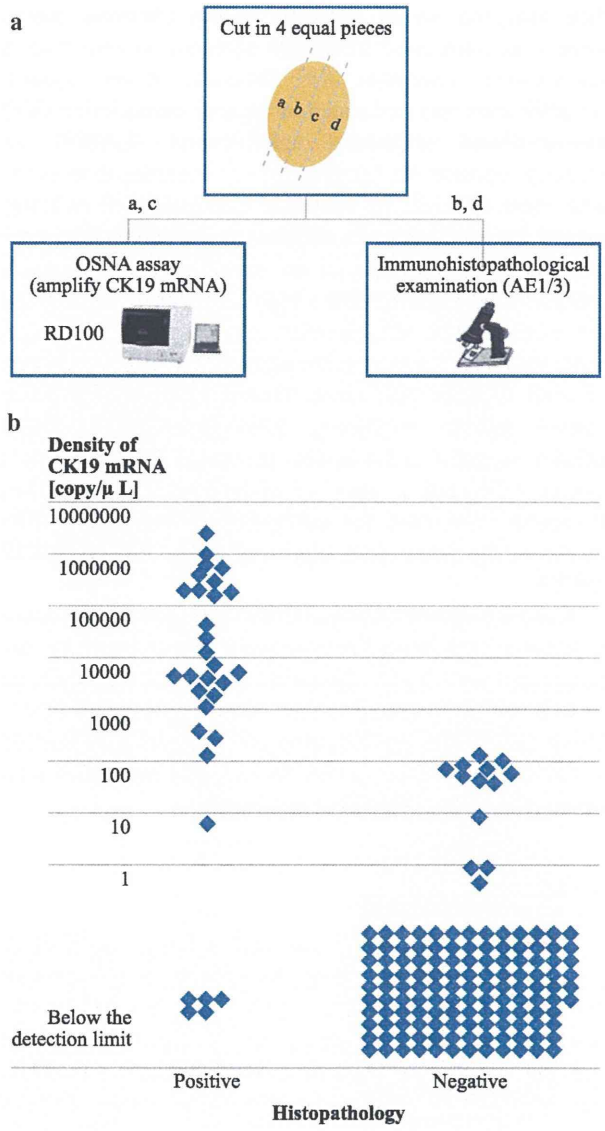

FIG. 1 **a** CLNs were cut into four equal pieces. Two of these pieces *a*, *c* were homogenized and centrifuged, and the supernatants were analyzed using the RD-100i system (Sysmex, Japan). The remaining 2 pieces *b*, *d* were examined immunohistochemically by the pathologists. **b** The levels of CK19 mRNA in OSNA assay according to histopathological diagnosis

The pathologists performing these procedures had no access to the results of the OSNA assay.

OSNA Assay

OSNA assay for CLNs was performed as described previously.[17] Briefly, two of the frozen pieces (a, c) were homogenized with 4 ml of buffer solution (Lynorhag; Sysmex, Kobe, Japan) and centrifuged at 10,000×*g* at room temperature. Two microliters of the supernatant were

then analyzed on an RD-100i system (Sysmex, Kobe, Japan), an automated molecular detection system with a ready-to-use Lynoamp Kit (Sysmex, Kobe, Japan). Amplification was performed by reverse transcription (RT) loop-mediated isothermal amplification (LAMP), as recently reported for CK19 mRNA.[23] Amplification products were detected by real-time monitoring of turbidity caused by an increase in magnesium pyrophosphate concentration, a by-product of the amplification reaction. A total of six primers implied a high degree of specificity for the reaction. The amplification process for each sample took less than 20 min, and the processing and amplification of three samples took about 30 min. A standard positive control sample containing 5,000 copies/μl of CK19 mRNA, regarded as the amount present in 2 mm^3 of breast cancer cells, and a negative control sample containing 0 copy/μl were used for calibration in each assay. The results of the assay were expressed as the level of CK19 mRNA.

A previous study classified OSNA levels in breast cancer as follows: a CK19 mRNA level less than 250 copies/μl was designated as (−); a level between 250 and 5,000 copies/μl as (+); and a level higher than 5,000 copies/μl as (++). Using this system, we compared the level and classification of CK19 mRNA from the OSNA assay for each CLN with immunohistochemical (IHC) outcomes.

Statistical Analyses

Diagnostic efficacy of the OSNA assay in HNSCC patients was evaluated using the area under the receiver operating characteristic curve (AUROC). We defined the results of the IHC diagnosis as the objective standard and those of the OSNA assay as the diagnostic test value. All statistical analyses were performed using STATA version 10 (STATA Corp., College Station, TX, USA), with two-sided P values of <0.05 considered statistically significant.

RESULTS

Patient Characteristics

Characteristics of the 56 patients are summarized in Table 1. Median age was 65 years (range 29–81), and male sex was predominant. In terms of T classification, almost all patients had T2 disease or worse. With regard to clinical CLNs, ~50 % of patients were N0 cases. In addition, tumors were located in the oral cavity in almost half of the patients. Approximately 80 % patients had undergone surgery at Fukushima Medical University or Gunma University.

TABLE 1 Characteristics of the 56 study patients

Characteristic	Value
Age, year, median (range)	65 (29–81)
Sex (%)	
Male	51 (91)
Female	5 (9)
T classification[a] (%)	
1	3 (5)
2	23 (41)
3	16 (29)
4a	14 (25)
N classification[a] (%)	
0	27 (48)
1	7 (13)
2a	4 (7)
2b	12 (21)
2c	5 (9)
3	1 (2)
Primary cancer site (%)	
Oral cavity	25 (44)
Oropharynx	5 (9)
Hypopharynx	15 (27)
Larynx	9 (16)
Maxillary sinus	1 (2)
Salivary	1 (2)
Institute (%)	
Fukushima Medical University	21 (38)
Gunma University	23 (41)
Kyorin University	8 (14)
Aichi Cancer Center	4 (7)

[a] According to the 7th edition of the Union for International Cancer Control tumor, node, metastasis staging system

Comparison of OSNA Assay with Histopathological Diagnosis

CK19 mRNA levels obtained using the OSNA assay ranged from less than the detection level to 24,00,000 copies/μl (Fig. 1b). Receiver operating characteristic curve (ROC) evaluation showed that OSNA assay had good discriminative power relative to histopathological diagnosis, and was highly useful in detecting pathological CLN metastasis in terms of the area under the ROC (AUROC 0.918; 95 % confidence interval [CI] 0.852–0.984; Fig. 2).

Cutoff Value of CK19 mRNA in OSNA Assay

The cutoff value for OSNA assay between histopathologically positive and negative CLNs in HNSCC patients was evaluated from the sensitivity, specificity, positive

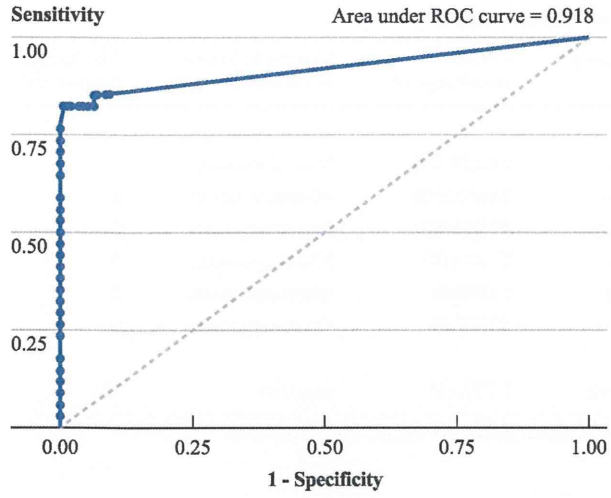

FIG. 2 Receiver operating characteristics (ROC) curve of CK19 mRNA as evaluated by OSNA assay according to histopathological examinations. The area under the ROC curve (AUROC) was 0.918 (95 % CI, 0.852–0.984)

likelihood ratio, and negative likelihood ratio of the serial cutoff values. According to the OSNA assay classification for breast cancer, 15 CLNs were designated as (++), 11 as (+), and 149 as (−). Sensitivity of this classification was 76.5 % (95 % CI 58.8–89.3 %) and specificity was 100 % (95 % CI 97.5–100.0 %). Table 2 shows the results with cutoffs other than 250 copies/μl. In this study, detection was optimum at a cutoff point of 131 copies/μl (sensitivity 82.9, 95 % CI, 66.4–93.4 %; specificity 99.3, 95 % CI, 96.1–100.0 %; negative predictive value 95.9, 95 % CI, 91.3–98.5 %; positive likelihood ratio 118.5; negative likelihood ratio 0.2). Detailed information for other serial cutoff values are shown in Supplemental Table 1.

Discordant Cases Between OSNA Assay and Histopathological Diagnosis

Using a cutoff point of 131 copies/μl CK19mRNA, seven discordant cases were observed between OSNA assay and histopathological diagnosis, of which six were pathologically positive for metastases but negative in OSNA assay, while one was pathologically negative for metastasis and positive in OSNA assay (Table 3). Four of the six pseudo-negative cases had clinical N2 disease.

Consistency of OSNA Assay Among Hospitals

We also evaluated the diagnostic value of OSNA assay according to hospital using the cutoff point of 131 copies/μl (Supplemental Table 2). Although all hospitals had good specificity, sensitivity at Aichi Cancer Center was lower than at the other hospitals.

Difference Between Head and Neck Cancer and Other Cancer Sites in OSNA Assay

Finally, we compared the sensitivity and specificity of OSNA assay in head and neck cancer with those in other cancer sites (Table 4). Although sensitivity in our cases was slightly lower than that in other cancer sites, specificity among sites was consistent.

DISCUSSION

In this study, we demonstrated that OSNA assay has high intraoperative diagnostic value for CLN metastasis in HNSCC patients. The cutoff value for CK19mRNA offering the highest detection in HNSCC patients appeared to differ from that in breast cancer patients. To our knowledge, this is the first report to evaluate the efficacy of OSNA assay in HNSCC patients.

To overcome problems of conventional intraoperative diagnosis in SNNS, several authors have investigated molecular-based metastasis detection systems using RT polymerase chain reaction (PCR) for tumor markers. However, these are more complicated and time-consuming than intraoperative techniques.[8,24] Further, RT-PCR is occasionally unreliable because of the presence of pseudogenes and contamination with benign epithelial cells. Ferris et al. recently reported that intraoperative quantitative real-time PCR assay can accurately detect CLN metastasis in HNSCC patients.[25] A LAMP assay has been used for the rapid detection of genes.[23] Incubation in this system is carried out at a constant temperature and the need for specialized equipment or expertise is eliminated. OSNA assay is another molecular-based metastasis detection system that adopts RT-LAMP assay, using CK19 as a single marker. CK19 is a representative epithelial marker which is widely expressed in human cancers, and is considered a promising marker with high sensitivity for the

TABLE 2 Effect of diagnostic value in the serial cutoff values of CK19mRNA in OSNA analysis

Copies/μl	Sensitivity		Specificity		LR	
	%	95 % CI	%	95 % CI	Positive	Negative
100	82.4	65.5–93.2	98.6	95.0–99.8	58.1	0.2
131	82.4	65.5–93.2	99.3	96.1–100.0	116.1	0.2
300	76.5	58.8–89.3	100.0	97.4–100.0	Not estimated	0.2

CI confidence interval, *LR* likelihood ratio

TABLE 3 CK19mRNA in seven discordant cases according to the histopathological examinations

Discordant findings (patient no.)	Age	Sex	Hospital	Site of primary disease	cTNM classification[a]	Histopathological examination	CK19mRNA (copies/μl)[b]
Pathology (positive), OSNA (negative)							
1	73	M	Gunma	Oral cavity	T4aN2cM0	Macrometastasis	0
2	66	M	Gunma	Oropharynx	T4aN2bM0	Macrometastasis	0
3	66	M	Gunma	Hypopharynx	T2N2bM0	Macrometastasis	0
4	65	M	Gunma	Oral cavity	T2N2bM0	Macrometastasis	0
5	29	M	Aichi	Oral cavity	T2N0M0	Macrometastasis	0
6	69	F	Fukushima	Oral cavity	T3N0M0	Micrometastasis	6
Pathology (negative), OSNA (positive)							
7	68	M	Fukushima	Hypopharynx	T3N1M0	Negative	131

[a] According to the 7th edition of the Union for International Cancer Control tumor, node, metastasis staging system

[b] CK19 mRNA 131 copies/μl was defined as the cutoff

TABLE 4 The impact of diagnostic value in OSNA analysis according to cancer site

Cancer site	Cutoff (copies/μl)	Sensitivity (%)	95 % CI	Specificity (%)	95 % CI
Head and neck	131	82.4	65.5–93.2	99.3	96.1–100.0
Breast					
Tamaki et al.[9]	250	95.0	75.1–99.9	97.1	91.8–99.4
Schem et al.[19]	250	98.1	93.3–99.8	89.0	84.3–92.7
Visser et al.[20]	250	95.3	86.9–99.0	94.7	91.3–97.0
Stomach[21]	250	88.9	75.9–96.3	96.6	91.5–99.0
Colorectal[22]	250	95.2	88.1–98.7	97.7	95.3–99.1

CI confidence interval

detection of lymph node metastases from various cancers, including HNSCC.[26–29] Although we demonstrated the efficacy of OSNA assay in HNSCC, its use in these patients nevertheless remains controversial.[30] Additionally, while we defined 131 copies/μl of CK19mRNA as a cutoff in HNSCC patients, results with this cutoff differed from those in other cancer sites. With regard to diagnostic value, intraoperative frozen section diagnosis has a sensitivity of 60–70 % in HNSCC patients, mainly as a result of the failure to detect micrometastasis.[8,9,15,16] The diagnostic value of OSNA assay in our present cases was greater than these values, however, supporting the efficacy of OSNA assay for intraoperative diagnosis in HNSCC patients. Additionally, the time needed for OSNA assay is approximately 30 min or less. For implementation of OSNA assay in SNNS, validation of this finding in larger HNSCC cohort is essential.

With regard to the discordancy between OSNA assay and IHC, it might be derived from a biased allocation of CLNs for two examinations by chance.

As OSNA assay in practical setting assess a whole lymph node and yields semiquantitative results, it is assumed to be avoidable in SNNS.

Our study had several strengths. First, it was conducted under a multicenter design. Second, because the performance of OSNA assay is constant, our results are likely reproducible in other hospitals.

Several limitations also warrant mention. First, approximately half of each CLN was provided for OSNA assay and the other half was used for histological analysis. The unavoidable allocation bias that this entailed, involving the localization of metastasis in CLN pieces, meant that discordance could not be avoided. Second, although we analyzed all clinical N stages in this study, OSNA assay also showed efficacy in N0 patients (data not shown). Third, the moderate sample size may have limited the study, necessitating its duplication in a larger scale cohort.

In conclusion, these findings suggest that OSNA assay has a high intraoperative diagnostic value for CLN metastasis in HNSCC patients. Optimum CK19mRNA cutoff value in HNSCC patients might differ from that in breast cancer patients. OSNA assay could be applied for the intraoperative diagnosis in the SNNS in HNSCC patients. A further large scale study to validate our results and establish the cutoff value to minimize the false omission rate is warranted.

ACKNOWLEDGMENT This research was supported by Grants-in-aid for Scientific Research (C) from the Japan Society for the Promotion of Science, and a Health and Labor Sciences Research Grant for Clinical Cancer Research (H21-Gannrinshou-Ippan-016) from the Ministry of Health, Labor and Welfare, Japan.

REFERENCES

1. Murer K, Huber GF, Haile SR, Stoeckli SJ. Comparison of morbidity between sentinel node biopsy and elective neck dissection for treatment of the n0 neck in patients with oral squamous cell carcinoma. *Head Neck.* 2011;33:1260–4.
2. Alkureishi LW, Ross GL, Shoaib T, Soutar DS, Robertson AG, Thompson R, et al. Sentinel node biopsy in head and neck squamous cell cancer: 5-year follow-up of a European multicenter trial. *Ann Surg Oncol.* 2010;17:2459–64.
3. Kohno N, Ohno Y, Kihara K, Kitahara S, Tamura E, Tanabe T, et al. Feasibility of sentinel lymph node radiolocalization in neck node-negative oral squamous cell carcinoma patients. *ORL J Otorhinolaryngol Relat Spec.* 2003;65:66–70.
4. Kosuda S, Kusano S, Kohno N, Ohno Y, Tanabe T, Kitahara S, et al. Feasibility and cost-effectiveness of sentinel lymph node radiolocalization in stage N0 head and neck cancer. *Arch Otolaryngol Head Neck Surg.* 2003;129:1105–9.
5. Matsuzuka T, Kano M, Ohtani I, Miura T, Shishido F, Omori K. Impact of sentinel node navigation technique for carcinoma of tongue with cervical node metastases. *Auris Nasus Larynx.* 2005; 32:59–63.
6. Terada A, Hasegawa Y, Goto M, Sato E, Hyodo I, Ogawa T, et al. Sentinel lymph node radiolocalization in clinically negative neck oral cancer. *Head Neck.* 2006;28:114–20.
7. Matsuzuka T, Kano M, Ogawa H, Miura T, Tada Y, Matsui T, et al. Sentinel node mapping for node positive oral cancer: potential to predict multiple metastasis. *Laryngoscope.* 2008;118: 646–9.
8. Terada A, Hasegawa Y, Yatabe Y, Hyodo I, Ogawa T, Hanai N, et al. Intraoperative diagnosis of cancer metastasis in sentinel lymph node of oral cancer patients. *Oral Oncol.* 2008;44:838–43.
9. Terada A, Hasegawa Y, Yatabe Y, Hanai N, Ozawa T, Hirakawa H, et al. Follow-up after intraoperative sentinel node biopsy of N0 neck oral cancer patients. *Eur Arch Otorhinolaryngol.* 2011; 268:429–35.
10. Yamauchi K, Fujioka Y, Kohno N. Sentinel node navigation surgery versus observation as a management strategy for early tongue carcinoma. *Head Neck.* 2012;34:568–72.
11. Yoshimoto S, Hasegawa Y, Matsuzuka T, Shiotani A, Takahashi K, Kohno N, et al. Sentinel node biopsy for oral and laryngopharyngeal squamous cell carcinoma: a retrospective study of 177 patients in Japan. *Auris Nasus Larynx.* 2012;39:65–70.
12. Ross GL, Soutar DS, Gordon MacDonald D, Shoaib T, Camilleri I, Roberton AG, et al. Sentinel node biopsy in head and neck cancer: preliminary results of a multicenter trial. *Ann Surg Oncol.* 2004;11:690–6.
13. Broglie MA, Haile SR, Stoeckli SJ. Long-term experience in sentinel node biopsy for early oral and oropharyngeal squamous cell carcinoma. *Ann Surg Oncol.* 2011;18:2732–8.
14. Civantos FJ, Zitsch RP, Schuller DE, Agrawal A, Smith RB, Nason R, et al. Sentinel lymph node biopsy accurately stages the regional lymph nodes for T1–T2 oral squamous cell carcinomas: results of a prospective multi-institutional trial. *J Clin Oncol.* 2010; 28:1395–400.
15. Rassekh CH, Johnson JT, Myers EN. Accuracy of intraoperative staging of the N0 neck in squamous cell carcinoma. *Laryngoscope.* 1995;105:1334–6.
16. Civantos FJ, Gomez C, Duque C, Pedroso F, Goodwin WJ, Weed DT, et al. Sentinel node biopsy in oral cavity cancer: correlation with PET scan and immunohistochemistry. *Head Neck.* 2003; 25:1–9.
17. Tsujimoto M, Nakabayashi K, Yoshidome K, Kaneko T, Iwase T, Akiyama F, et al. One-step nucleic acid amplification for intraoperative detection of lymph node metastasis in breast cancer patients. *Clin Cancer Res.* 2007;13:4807–16.
18. Tamaki Y, Akiyama F, Iwase T, Kaneko T, Tsuda H, Sato K, et al. Molecular detection of lymph node metastases in breast cancer patients: results of a multicenter trial using the one-step nucleic acid amplification assay. *Clin Cancer Res.* 2009;15: 2879–84.
19. Schem C, Maass N, Bauerschlag DO, Carstensen MH, Loning T, Roder C, et al. One-step nucleic acid amplification—a molecular method for the detection of lymph node metastases in breast cancer patients; results of the German study group. *Virchows Arch.* 2009;454:203–10.
20. Visser M, Jiwa M, Horstman A, Brink AA, Pol RP, van Diest P, et al. Intra-operative rapid diagnostic method based on CK19 mRNA expression for the detection of lymph node metastases in breast cancer. *Int J Cancer.* 2008;122:2562–7.
21. Yaguchi Y, Sugasawa H, Tsujimoto H, Takata H, Nakabayashi K, Ichikura T, et al. One-step nucleic acid amplification (OSNA) for the application of sentinel node concept in gastric cancer. *Ann Surg Oncol.* 2011;18:2289–96.
22. Yamamoto H, Sekimoto M, Oya M, Yamamoto N, Konishi F, Sasaki J, et al. OSNA-based novel molecular testing for lymph node metastases in colorectal cancer patients: results from a multicenter clinical performance study in Japan. *Ann Surg Oncol.* 2011;18:1891–8.
23. Notomi T, Okayama H, Masubuchi H, Yonekawa T, Watanabe K, Amino N, et al. Loop-mediated isothermal amplification of DNA. *Nucleic Acids Res.* 2000;28:E63.
24. Germani RM, Civantos FJ, Elgart G, Roberts B, Franzmann EJ. Molecular markers of micrometastasis in oral cavity carcinomas. *Otolaryngol Head Neck Surg.* 2009;141:52–8.
25. Ferris RL, Xi L, Seethala RR, Chan J, Desai S, Hoch B, et al. Intraoperative qRT-PCR for detection of lymph node metastasis in head and neck cancer. *Clin Cancer Res.* 2011;17:1858–66.
26. Tao L, Lefevre M, Ricci S, Saintigny P, Callard P, Perie S, et al. Detection of occult carcinomatous diffusion in lymph nodes from head and neck squamous cell carcinoma using real-time RT-PCR detection of cytokeratin 19 mRNA. *Br J Cancer.* 2006;94: 1164–9.
27. Zhong LP, Zhao SF, Chen GF, Ping FY, Xu ZF, Hu JA. Increased levels of CK19 mRNA in oral squamous cell carcinoma tissue detected by relative quantification with real-time polymerase chain reaction. *Arch Oral Biol.* 2006;51:1112–9.
28. Xu Y, Zhao X, Guan M, Li B, Zhou Y, Zhou F. Determination of lymph node micrometastases in patients with supraglottic carcinoma. *Acta Otolaryngol.* 2007;127:1188–95.
29. Zhong LP, Chen WT, Zhang CP, Zhang ZY. Increased CK19 expression correlated with pathologic differentiation grade and prognosis in oral squamous cell carcinoma patients. *Oral Surg Oral Med Oral Pathol Oral Radiol Endod.* 2007;104:377–84.
30. Yamauchi K, Fujioka Y, Kogashiwa Y, Kohno N. Quantitative expression study of four cytokeratins and p63 in squamous cell carcinoma of the tongue: suitability for sentinel node navigation surgery using one-step nucleic acid amplification. *J Clin Pathol.* 2011;64:875–9.

Ann Nucl Med (2012) 26:281–285
DOI 10.1007/s12149-011-0565-0

SHORT COMMUNICATION

Comparison of animal studies between interstitial magnetic resonance lymphography and radiocolloid SPECT/CT lymphoscintigraphy in the head and neck region

Naoto Kitamura · Shigeru Kosuda · Koji Araki · Masayuki Tomifuji · Daisuke Mizokami · Akihiro Shiotani · Hiroshi Shinmoto · Hirofumi Fujii · Kiyoshi Ichihara

Received: 16 August 2011 / Accepted: 15 December 2011 / Published online: 12 January 2012

Abstract
Objective To comparatively assess two techniques, radiocolloid SPECT/CT lymphoscintigraphy and interstitial MR lymphography using SPIO and gadoxetate disodium, in animal models.
Materials and methods We used twenty one 8-week-old male nude mice of strain BALB/c Slc-nu/nu, weighing 23–27 g. The 4.7-T MRI equipment was used to detect the SNs. T2*WI of gradient-echo sequences was acquired sequentially up to 24 h after administering SPIO, ferucarbotran. T1WI was acquired sequentially up to 80 min after administering gadoxetate disodium. ^{99m}Tc-phytate SPECT/CT lymphoscintigraphy was taken at 30 min after the injection to detect the SNs using animal-dedicated whole-body SPECT/CT hybrid scanner. The injection was submucosally performed in the right tongue margin of each mouse. Reading performances concerning SN visualization and its quality on interstitial MR lymphogram and SPECT/CT lymphoscintigram were performed by 3 radiologists.
Results The SN intensities were 0.43 for the right, 0.61 for the left at 30 min after ferucarbotran injection, with gradual decrease in intensity, and 1.43 for the right, 1.33 for the left at 10 min after gadoxetate disodium injection with a fast decrease in intensity. The base value of 1.0 was at pre-examination. The mean numbers of lymph nodes visualized were 4.00 nodes for on SPECT/CT lymphoscintigram and 2.0 for interstitial MR lymphogram. There was a statistically significant difference in the mean scores between SPECT/CT lymphoscintigraphy and interstitial MR lymphography (two factor mixed design with repeated measures on one factor: $p < 0.0002$).
Conclusions In our comparative study using mice, the results of radiocolloid SPECT/CT lymphoscintigraphy were superior to those of interstitial MR lymphography, while both SPIO and gadoxetate disodium have a potential of being employed for sentinel node navigation surgery by interstitial MR lymphography in the head and neck region.

Keywords Sentinel node · ^{99m}Tc-phytate · Lymphoscintigraphy · SPECT/CT · Interstitial MR lymphography

N. Kitamura
Department of Radiotherapy, Keio University School of Medicine, 35 Shinanomachi, Shinjuku, Tokyo, Japan

S. Kosuda (✉) · H. Shinmoto
Department of Radiology, National Defense Medical College, 3-2 Namiki, Tokorozawa, Saitama 359-8513, Japan
e-mail: nucleark@ndmc.ac.jp

K. Araki · M. Tomifuji · D. Mizokami · A. Shiotani
Department of Otolaryngology, National Defense Medical College, 3-2 Namiki, Tokorozawa, Saitama, Japan

H. Fujii
Functional Imaging Division, Research Center for Innovative Oncology, National Cancer Center Hospital East, 6-5-1 Kashiwanoha, Kashiwa, Chiba, Japan

K. Ichihara
Department of Clinical Laboratory Science, Faculty of Health Science, Yamaguchi University Graduate School of Medicine, 1-1-1 Minamikogushi, Ube, Yamaguchi, Japan

Introduction

There are several reports on the application of sentinel lymph node biopsy (SLNB) using radiocolloid for the management of head and neck cancer patients [1–4]. SLNB

has become a useful tool. This technique allows head and neck surgeons to avoid the futile and unnecessary step of neck dissection, and reduce the incidence of postoperative morbidities such as shoulder pain.

However, SLNB using ^{99m}Tc-radiocolloid has some drawbacks. Shine-through phenomenon encountered during the use of these compounds generally hampers sentinel node (SN) detection when the SN exists near the injection site of the ^{99m}Tc-radiocolloid.

Superparamagnetic iron oxides (SPIO) are nanoparticles, which get incorporated into macrophages and other phagocytic cells, and used as macrophage imaging agents [5, 6]. SPIOs generate a strong negative contrast in T2 and T2* MR images. There are the documentations that interstitial MR lymphography had excellent results for the detection of SNs [7, 8].

The objective of this study was to comparatively assess two techniques, radiocolloid SPECT/CT lymphoscintigraphy and interstitial MR lymphography using SPIO and gadoxetate disodium, in animal models. To the best of our knowledge, this is the first study concerning a comparison between the two techniques in the head and neck region.

Materials and methods

All procedures used in this study adhered to the institutional guidelines for the care and use of experimental animals. We used twenty one 8-week-old male nude mice of strain BALB/c Slc-nu/nu, weighing 23–27 g. The mice were anesthetized by isoflurane and tethered to restrict physical movement before the experiment. Respiratory gating was not performed. Contrast medium or radioactive tracer was not administered in three mice that were used as a control.

SPECT/CT lymphoscintigraphy

^{99m}Tc-phytate of 0.02 mL, 7.4 MBq, was submucosally injected into the right side margin of the tongue in each of six mice. Lymphoscintigraphic imaging was taken at 30 min after the injection to detect the SNs. Acquisition time was 30 min. We used the in vivo animal-dedicated whole-body SPECT/CT hybrid scanner, NanoSPECT/CT® (BIOSCAN Mediso., Washington, DC, USA). The SPECT apparatus we used had three detectors equipped with 9-hole multi-pinhole collimators. A hole was 1.4 mm in diameter. CT images were taken with a helical CT in the setting of tube voltage of 45 kV and tube current of 177 microA. Assessment of the optimal timing for visualization of lymph node was not performed because an acquisition technique for radiocolloid lymphoscintigraphy has established in head and neck region [1–4].

Interstitial MR lymphography

We used the Varian Unity INOVA 4.7-T MRI equipment (Varian Co., Palo Alto, CA, USA) to detect the SNs. The following coils were used: gradient coil: 6.5 gauss/cm; transmitting coil: varian volume coil, 16 cm Φ; and receiving coil: handmade surface coil, 5 cm Φ.

The pulse sequences were as follows: 3D gradient-echo: TR/TE = 0.02/0.004 s, field of view (FOV) = 80 × 40 × 40 mm, matrix size = 128 × 64 × 64, flip angle = 8 degrees; spin-echo, T1-weighted image (T1WI): TR/TE = 0.4/0.014 s, FOV = 40 × 40 mm, matrix size = 256 × 256, slice thickness 1.3 mm, gradient-echo, T2*-weighted image (T2*WI): TR/TE = 0.02/0.008 s, FOV = 40 × 40 mm, matrix size = 256 × 256, slice thickness = 1.3 mm, flip angle = 32°.

The free induction decay (FID) data collected by the MRI equipment were displayed in a 16-bit format; the data were converted using the Fourier algorithm and the original MATLAB program (MathWorks Inc., Natick, MA, USA).

The T2*WI of gradient-echo sequences was acquired sequentially at 30, 80, 110 min and 24 h after administering submucosal injection of the SPIO ferucarbotran (Resovist®) which was provided by Bayer Schering Pharma AG (Berlin, Germany). The injections were submucosally administered in the right side margins of the tongues of six mice using a 29G needle and a 1 mL syringe; 0.01 mL, 0.279 mg iron of ferucarbotran. The conventional T1WI was acquired sequentially at 10, 20, 30, 40, 50, 60, 70, and 80 min after administering a submucosal injection of gadoxetate disodium, which was provided by Bayer Schering Pharma AG. The gadoxetate disodium of 0.01 mL, 0.363 mg, was submucosally injected into each of other six mice in the same way as a ferucarbotran injection. The injected dose and volume were determined according to the previous animal studies [7, 9] and a personal contact at the head and neck sentinel node navigation surgery meeting, which was held by a grant from the 2009 Health, Welfare, Labor, Science Ministry Research Subsidy.

The regions of interest (ROI) on the display images were carefully defined over the right and left submandibular lymph nodes and the cervical muscular tissue used as the background, referring to a color anatomy atlas [12–14]. The time–intensity graphs were generated on each ROI. In addition, these data files were analyzed by a commercially available software, namely ImageJ. The intensity values of the ROIs were adjusted by dividing them with the background intensity values. The intensity on the non-contrast MR image was defined as 1.0 in the studies using ferucarbotran and gadoxetate disodium. The time–intensity graphs were created using the above-mentioned data. The optimal time of obtaining a good-quality image of SN after

the interstitial injection of the contrast agents, ferucarbotran and gadoxetate disodium, was also assessed.

Reading performances concerning lymph node visualization and its quality on interstitial MR lymphogram and SPECT/CT lymphoscintigram were performed by 3 radiologists with experience of more than 10 years. Image quality of interstitial MR lymphography was compared with that of the control mice.

In interstitial MR lymphography and SPECT/CT lymphoscintigraphy, lymph nodes (SNs) visualization was classified into 4 grades, poor, fair, good, and excellent, comparing the background. The grades were visually and subjectively scored by the three radiologist readers.

For comparison of the grades of lymph node visualization by three radiologist readers, two-factor mixed design with repeated measures on one factor was performed using SPSS software (SPSS Inc.), and P value less than 0.05 was considerably statistically significant.

Results

SNs were well visualized in a color display mode on SPECT/CT fusion lymphoscintigraphy. The numbers of SNs visualized on SPECT/CT lymphoscintigrams were 3, 3, 5, 6, 3 and 4 in each mouse (mean: 4.00 nodes). Sixteen nodes were visualized in the right side and 8 in the left side.

The normal submandibular nodes with slightly low signal intensity were seen on T2*WI in the control mouse. In interstitial MR lymphography using ferucarbotran, T2*WI showed the right and left submandibular nodes alone as low-intensity signals from 30 min to 24 h after the injection. No other nodes except the submandibular nodes were visualized on the T2*WI. However, T1WI showed the right and left submandibular nodes alone as high-intensity signals from 10 min to 24 h after gadoxetate disodium injection, although the intensity was gradually decreased. Shine-through phenomenon was observed at the injection site on both T2*WI by a ferucarbotran injection and T1WI by a gadoxetate disodium injection.

The time–intensity graph obtained using T2*WI data suggested that the SN intensity at 30 min after ferucarbotran injection (right: 0.43, left: 0.61, the base value of 1.0 at the pre-examination) was approximately half as compared to that before injection, and the SNs' intensities were slightly decreased with the lapse of time was up to 24 h after the ferucarbotran injection. The SN intensities of the right nodes were less than those of the left nodes (Fig. 1). The time–intensity graph obtained using T1WI data showed high density areas after the gadoxetate disodium injection, with the highest intensity (right: 1.43, left: 1.33, the base value of 1.0 at the pre-examination) being observed at 10 min after the injection, which gradually decreased up to 80 min after the injection. The SN intensities of the right nodes were higher than those on the left nodes (Fig. 2).

Interstitial MR lymphography depicted only two nodes in each of lymphograms by the ferucarbotran injection or gadoxetate disodium injection (mean: 2.0 nodes) (Table 1). The highest radioactive nodes on SPECT/CT were consistent with the node detected by interstitial MR lymphography.

The three readers' grades of interstitial MR lymphography and SPECT/CT fusion lymphoscintigraphy concerning SN visualization are also shown in Table 1. The results of SPECT/CT fusion lymphoscintigraphy were superior to those of interstitial MR lymphography according to the three readers' performances (Table 1; Fig. 3). The mean scores by three readers were 1.44 in SPIO interstitial MR, 1.67 in gadoxetate disodium interstitial MR lymphography, and 2.67 in SPECT/CT lymphoscintigraphy. Thus, there was a statistically significant difference in the mean scores between SPECT/CT lymphoscintigraphy and interstitial MR lymphography (two-factor mixed design with repeated measures on one factor: $p < 0.0002$).

Discussion

Although the usefulness of SLNB in clinical N0 patients with head and neck cancer has been gradually recognized in the clinical setting, SLNB has not yet been employed worldwide, except for a few institutes. In addition, there are some concerns about SLNB using ^{99m}Tc-radiocolloid. Especially, the submental and submandibular lymph nodes are greatly affected by shine-through phenomenon when the patient has oral floor cancer, tongue cancer, or gingival cancer. Appropriate training and experience are required for performing SLNB using ^{99m}Tc-radiocolloid. The false-negative rate of SLNB in tongue cancer patients is relatively high, approximately 8%, which could impair feasibility of SLNB and might conflict with SN concept [15].

MRI SPIO contrast, ferucarbotran, was developed for liver imaging. The particle size of ferucarbotran is approximately 60–200 nm [16]. This size is optimal for incorporation into the Kupffer cells in the liver, resulting in a conspicuously lower signal intensity on T2WI and T2*WI. Many investigators have documented the usefulness of SPIO for detecting intrahepatic tumors.

In our series, the bilateral submandibular lymph nodes could be detected by both an SPIO, ferucarbotran and an MR contrast agent, gadoxetate disodium using a 4.7-T MRI system. There is a possibility that an MRI system with from 1.0 to 3.0 T can be used for interstitial MR lymphography [8, 9]. The right submandibular node was presumably an SN because the interstitial injections were administered in the right tongue margin, and the right node was more

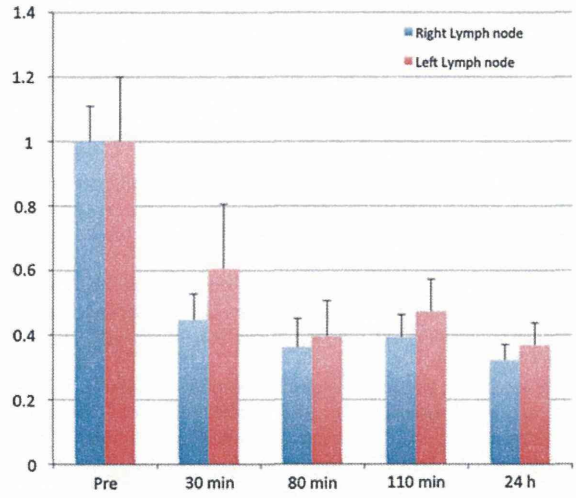

Fig. 1 Ferucarbotran (SPIO) was submucosally injected at the right margin of the tongue. Time–intensity *graphs* were generated on the regions of interest (ROI) created over the right and left submandibular lymph nodes after the injection

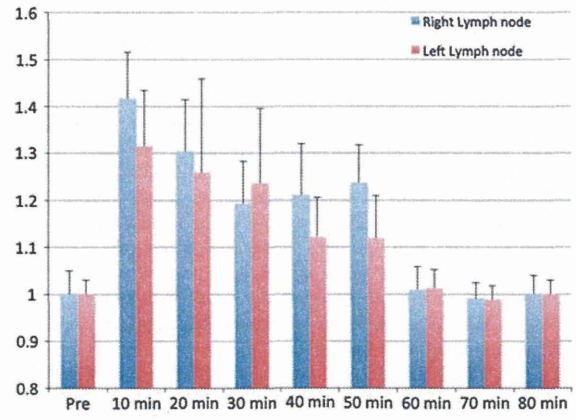

Fig. 2 Gadoxetate disodium was submucosally injected at the right margin of the tongue. Time–intensity *graphs* were generated on the regions of interest (ROI) created over the right and left submandibular lymph nodes after the injection

prominently visualized in all pulse sequence images and on the time–intensity graphs. The submandibular node is one of the SNs, which frequently harbor micrometastasis in tongue cancer patients [1–4, 15, 17].

Recently, gadoxetate disodium, which is a variant of gadolinium-diethylene triamine-pentaacetic acid (Gd-DTPA), containing a lipophilic ethyl-oxy-benzyl group, has been developed as a hepatocyte-specific agent [18]. Unlike SPIO, gadoxetate disodium is not composed of nanoparticles. Gadoxetate disodium was chosen in our study because it has a potential of an excellent contrast for interstitial MR lymphography [9]. The observed optimal timing for visualization of lymph node was almost concordant with the timing of the previous studies [7, 9].

The image quality obtained with gadoxetate disodium was superior to that obtained with ferucarbotran owing to the positive image visualization of the nodes (Table 1); however, imaging with gadoxetate disodium had a drawback of rapid washout. Surgeons will fail to use a sensitive handheld magnetometer ex vivo at operation if contrast has rapid washout from a SN. Reversely, the rapid kinetics will enable us to repeat interstitial MR lymphography. In contrast to gadoxetate disodium, the degree of incorporation of SPIO and their retention in the cells are dose-dependent and these compounds accumulate slowly and continuously over more than 5 h [10]. As compared to USPIO, SPIO exhibited a higher uptake rate, probably owing to their

Table 1 The three readers' grades of interstitial MR lymphography and SPECT/CT fusion lymphoscintigraphy concerning SN visualization

Readers	MRI		SPECT/CT
	Ferucarbotran Mouse 1, 2, 3, 4, 5, 6	Gadoxetate disodium Mouse 7, 8, 9, 10, 11, 12	Mouse 13, 14, 15, 16, 17, 18
Reader A	G G G G F F	G G F G G G	E E G G E G
Reader B	F F G F F F	G G G F F G	E E G G E E
Reader C	F G G G F F	G G F F F G	E E E G E E

F fair = 1, *G* good = 2, *E* excellent = 3

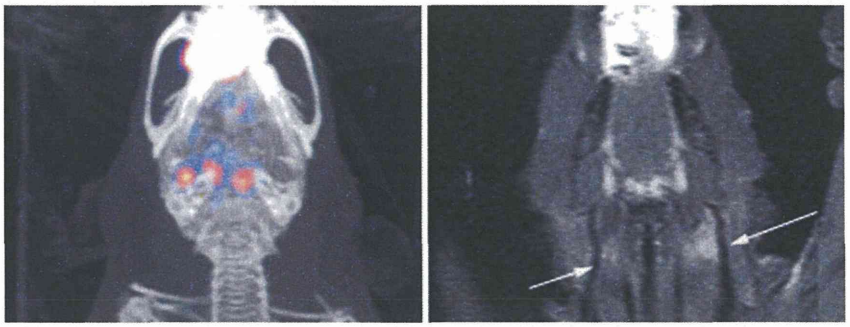

Fig. 3 SPECT/CT fusion lymphoscintigram (*left*) depicts SNs more clearly than interstitial MR lymphography using gadoxetate disodium (*right*). *Arrows* show the submandibular glands

larger particle size and more negative charge making them more attractive for detecting cells with high phagocytic activity [11, 19].

Shine-through phenomenon was also observed in interstitial MR lymphography. A streak artifact was seen around the injection site, probably because we used a considerable dose of the contrast medium in each mouse. The optimal dose for interstitial MR lymphography per mouse remains to be determined. We used undiluted contrast media. Dilution of SPIO with saline has a possibility of decreasing the streak artifact.

Furthermore, the injection site and adjacent tissues may be affected adversely because a large amount of contrast media is injected into the submucosal tissue. However, localized side effect, if any, is not a matter of anxiety since the injection site and its adjacent tissues are removed together with the primary lesion.

There may be a criticism that comparison of different imaging is always challenging and visual grading by clinical researchers provides a clue on image quality. However, three readers evaluated SN visualization and its image quality in interstitial MR lymphography and SPECT/CT lymphoscintigraphy, which was superior to interstitial MR lymphography in the readers' scores. The mean number of lymph nodes visualized was 2.0 in interstitial MR lymphography and 4.00 in SPECT/CT lymphoscintigraphy. A node with the maximum counts or the first echelon node is not always a SN [14]. Therefore, interstitial MR lymphography has a possibility of missing SN. It is easy to confirm the true SN if the lymphatic route to the SN is visualized because two or more lymphatic channels, which drain tracer simultaneously, can exist. Furthermore, we are planning to perform a new comparative study using blue dye, SPIO, and radiocolloid.

We conclude that in our comparative study using mice, the results of radiocolloid SPECT/CT lymphoscintigraphy were superior to those of interstitial MR lymphography, while both SPIO and gadoxetate disodium have a potential of being employed for SNNS by interstitial MR lymphography in the head and neck region.

Acknowledgments This study was funded by a grant from the 2009 Health, Welfare, Labor, Science Ministry Research Subsidy (2009-cancer clinical general, 016). The authors are indebted to the BioView Co. for the invaluable technical assistance and skills.

References

1. Civantos FJ, Stoeckli SJ, Takes RP, Woolgar JA, de Bree R, Paleri V, et al. What is the role of sentinel lymph node biopsy in the management of oral cancer in 2010? Eur Arch Otorhinolaryngol. 2010;267:839–44.
2. Stoecki SJ, Alkureishi LW, Ross GL. Sentinel node biopsy for early oral and oropharyngeal squamous cell carcinoma. Eur Arch Otorhinolaryngol. 2009;266:787–93.
3. Stoeckli SJ, Pfaltz M, Ross GL, Steinert HC, MacDonald DG, Wittekind C, et al. The second international conference on sentinel node biopsy in mucosal head and neck cancer. Ann Surg Oncol. 2005;12:919–24.
4. Paleri V, Rees G, Arullendran P, Shoaib T, Krishman S. Sentinel lymph node biopsy in squamous cell cancer of the oral cavity and oral pharynx: a diagnostic meta-analysis. Head Neck. 2005;27:739–47.
5. Stark DD, Weissleder R, Elizondo G, Hahn PF, Saini S, Todd LE, et al. Superparamagnetic iron oxide: clinical applications as a contrast agent for MR imaging of the liver. Radiology. 1988;168:297–301.
6. Weissleder R, Hahn PF, Stark DD, Elizondo G, Saini S, Todd LE, et al. Superparamagnetic iron oxide: enhanced detection of splenic tumors with MR imaging. Radiology. 1988;169:399–403.
7. Torchia MG, Nason R, Danzinger R, Lewis JM, Thlivertis JA. Interstitial MR lymphography for the detection of sentinel lymph nodes. J Surg Oncol. 2001;78:151–6.
8. Nakagawa T, Minamiya Y, Katayose Y, Saito H, Taguchi K, Imano H, et al. A novel method for sentinel lymph node mapping using magnetite in patients with non-small cell lung cancer. J Thorac Cardiovasc Surg. 2003;126:563–7.
9. Sheng F, Inoue Y, Kiryu S, Watanabe M, Ohtomo K. Interstitial MR lymphography in mice with gadopentetate dimeglumine and gadoxetate disodium. J Magn Reson Imaging. 2011;33:490–7.
10. Raynal I, Prigent P, Peyramaure S, Najid A, Rebuzzi C, Corot C. Macrophage endocytosis of superparamagnetic iron oxide nanoparticles. Mechanisms and comparison of ferumoxides and ferumoxtran-10. Invest Radiol. 2004;39:56–63.
11. Sun R, Dittrich J, Le-Huu M, Mueller MM, Bedke MM, Kartenbeck J, et al. Physical and biological characterization of superparamagnetic iron oxide- and ultrasmall superparamagnetic iron oxide-labeled cells. A comparison. Invest Radiol. 2005;40:504–13.
12. Hayakawa T, Iwaki T. A color atlas of sectional anatomy of the rat. Tokyo: Addthree; 2008. p. 18–30. (in Japanese).
13. Vogl TJ, Mack MG, Juergens M, Stark M, Pegios W, Bergman C, et al. MR diagnosis of head and neck tumors: comparison of contrast enhancement with triple-dose gadodiamide and standard-dose gadopentetate dimeglumine in the same patients. AJR Am J Roentgenol. 1994;163:425–32.
14. Carroll KW, Feller JF, Tirman PF. Useful internal standards for distinguishing infiltrative marrow pathology from hematopoietic marrow at MRI. J Magn Reson Imaging. 1997;7:394–8.
15. Terada A, Hasegawa Y, Goto M, Sato E, Hyodo I, Ogawa T, et al. Sentinel lymph node radiolocalization in clinically negative neck oral cancer. Head Neck. 2006;28:114–20.
16. Bach-Gansmo T, Fahlvik AK, Ericsson A, Hemmingsson A. Superparamagnetic iron oxide for liver imaging. Comparison among three different preparations. Invest Radiol. 1994;29:339–44.
17. Kosuda S, Kusano S, Kohno N, Ohno Y, Tanabe T, Kitahara S, et al. Feasibility and cost-effectiveness of sentinel lymph node radiolocalization in stage N0 head and neck cancer. Arch Otolaryngol Head Neck Surg. 2003;129:1105–9.
18. Van Beers BE, Grandin C, Pauwels S, Mottet I, Goudemant JF, Delos M, et al. Gd-EOB-DTPA enhancement pattern of hepatocellular carcinomas in rats: comparison with Tc-99m-IDA uptake. J Magn Reson Imaging. 1994;4:351–4.
19. Raynal I, Prigent P, Peyramaure S, Najid A, Rebuzzi C, Corot C. Macrophage endocytosis of superparamagnetic iron oxide nanoparticles. Invest Radiol. 2004;39:56–63.